ChemPhysChem

ChemPhysChem
Chemistry Europe
European Chemical Societies Publishing

RESEARCH ARTICLE OPEN ACCESS

Mechanosynthesis of Layered Double Perovskites with Aromatic Spacer Cations for Lead-Free Thin-Film Opto(electro)ionics

Maryam Ghasemi[1] | Gianluca Bravetti[2] | Michalis Loizos[3] | Marinos Tountas[3] | Ghewa AlSabeh[2,4] | Mahesh Kumar[5] | Emmanuel Kymakis[3,6] | Konstantinos Rogdakis[3,6] | Mohammad Reza Golobostanfard[1] | Jovana V. Milić[1,2]

[1]Department of Chemistry, University of Turku, Turku, Finland | [2]Adolphe Merkle Institute, University of Fribourg, Fribourg, Switzerland | [3]Department of Electrical & Computer Engineering, Hellenic Mediterranean University (HMU), Heraklion, Greece | [4]Laboratory of Photonics and Interfaces, Ecole Polytechnique Fédérale de Lausanne, Lausanne, Switzerland | [5]Department of Electrical Engineering, Indian Institute of Technology Jodhpur, Jodhpur, India | [6]Institute of Emerging Technologies, University Research and Innovation Center (HMU), Heraklion, Crete, Greece

Correspondence: Konstantinos Rogdakis (krogdakis@hmu.gr) | Mohammad Reza Golobostanfard (mohammadreza.golobostanfard@utu.fi) | Jovana V. Milić (jovana.milic@utu.fi)

Received: 20 October 2025 | **Revised:** 22 December 2025 | **Accepted:** 13 January 2026

Keywords: layered double perovskites | lead-free opto(electro)ionics | mechanosynthesis | resistive switching | thin film fabrication

ABSTRACT

In the quest for stable, eco-friendly, lead-free halide perovskites, layered double perovskite semiconductors are promising derivatives that remain underexploited. We demonstrate the use of mechanosynthesis to access these materials for silver(I) and bismuth(III) analogues incorporating benzylammonium and 1,4-phenylenedimethylammonium bromide cations in Ruddlesden–Popper and Dion–Jacobson phases, respectively. Their thin films were fabricated and analysed by a combination of techniques, demonstrating the potential use in thin-film opto(electro)ionics.

1 | Introduction

Lead-based metal halide perovskites have become one of the leading solution-processed thin-film semiconductors in optoelectronics, challenging state-of-the-art technologies [1]. These systems are based on the canonical ABX_3 perovskite structure where A, the central cation, can be either Cs^+, methylammonium (MA^+, $CH_3NH_3^+$) or formamidinium (FA^+, $(H_2N)_2CH^+$), B is typically divalent Pb^{2+}, and X is a halide anion (I^-, Br^-, or Cl^-; Figure 1). Solution-processed metal-halide perovskites are relatively soft crystalline materials featuring exceptional performance across various opto(electro)ionic devices, which is attributed to their direct bandgap, high absorption coefficient, long-range charge diffusion, high dielectric constant, and outstanding carrier mobility [2–4]. Despite their remarkable characteristics, however, they are mixed ionic-electronic conductors that are reactive to oxygen and moisture, which contributes to their instability under environmental conditions and during voltage bias, irradiation, and temperature changes [5–7]. This setback has stimulated various interfacial functionalisations, compositional engineering, and encapsulation strategies [8–12]. In addition, the toxicity of lead poses a major issue for the application, particularly when large-scale deployment is considered, presenting substantial health and environmental risks [13–15]. Therefore, lead-free and other perovskite-inspired materials have attracted considerable attention [16–18]. To this end, Sn^{2+} provided a suitable alternative [19], although Sn perovskites exhibit poor stability due to the rapid oxidation that affects their structure [16, 19]. A promising option emerged in the form of double perovskites, which rely on monovalent and trivalent metal cations replacing divalent metals (Pb^{2+}) in the crystal structure with the general formula $A_2B^+B^{3+}X_6$ [20–23]. Recent breakthroughs suggested that double perovskites with monovalent Ag^+ cation and the trivalent Bi^{3+} cation were promising candidates for lead-free perovskite solar

Maryam Ghasemi, Gianluca Bravetti, and Michalis Loizos contributed equally to this study.

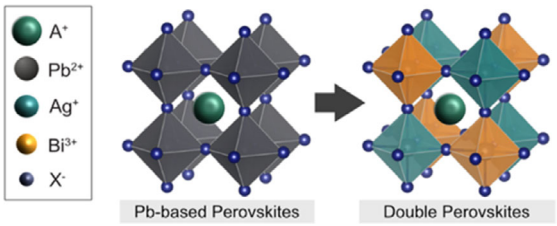

FIGURE 1 | Schematic of ABX_3 metal halide perovskite structure (B = Pb^{2+}; Ag^+, Bi^{3+}; X = I^-, Br^-, or Cl^-).

cells [24–26], even though $Cs_2AgBiBr_6$ has a large indirect bandgap [25, 27–29] and, therefore, the corresponding solar cells exhibit poor solar-to-electric power conversion efficiency [30]. A strategy to overcome the indirect bandgap and tailor the material properties is to develop layered derivatives of halide double perovskites through the introduction of large organic spacer cations [31]. This leads to the formation of two most common classes of layered double perovskites, the so-called Ruddlesden–Popper (RP) and Dion–Jacobson (DJ) phases templated by various alkylammonium cations [32–36]. In RP perovskites, the perovskite layers are displaced along the in-plane direction, involving mostly monofunctional spacers. In contrast, DJ perovskite phases are commonly based on bifunctional cations that connect the aligned neighbouring perovskite slabs (Figure 2). Despite their potential to enable more efficient and stable lead-free perovskite materials and devices, this class of low-dimensional materials remains underexploited to date [36].

Within the plethora of synthetic techniques to access halide perovskite materials, mechanosynthesis [37–40] presents a versatile approach based on a solid-state reaction at ambient temperature using mechanical energy, such as via ball milling [41]. This versatile approach can circumvent the solubility issue of the precursors while contributing to the crystallinity of the resulting materials [42]. Such a method offers notable advantages in reaction time and resource consumption, resulting in a combination of simplicity with an environmentally friendly solvent-free synthesis. It has been shown that mechanosynthesis is feasible under mild ambient conditions, owing to the soft crystalline nature of halide perovskites. However, it has been unexploited in the preparation of layered double perovskites, despite the potential to access these materials more readily and expand their scope [43].

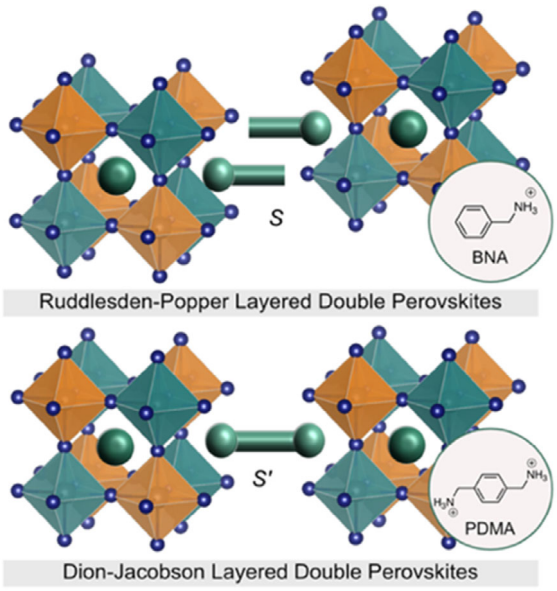

FIGURE 2 | Structural representation of RP (top) and DJ (bottom) layered double perovskite phases incorporating organic cations (S, S') in this study, i.e., benzylammonium (BNA) and 1,4-phenylenedimethylammonium (PDMA), based on $(BNA)_4A_{2(n-1)}(AgBi)_nBr_{2(3n+1)}$ and $(PDMA)_2A_{2(n-1)}(AgBi)_nBr_{2(3n+1)}$ compositions (representative $n = 2$ phases are illustrated with central A cations as green spheres).

In this work, we investigated RP and DJ layered double perovskite bromide phases incorporating benzylammonium (BNA) and 1,4-phenylenedimethylammonium (PDMA) organic spacers, which were accessed by using mechanosynthesis under ambient conditions. While various layered double perovskite compositions have been reported, we focus on AgBiX-based systems, considering their promise in opto(electro)ionics [36, 44]. Thin films were characterised using a combination of structural and optoelectronic techniques, demonstrating structural characteristics and behaviour typical of layered halide perovskite structures, highlighting mechanosynthesis as an effective tool for accessing layered halide double perovskites and their thin films. This offers a promising strategy to realise the potential of lead-free perovskites in opto(electro)ionic devices, as illustrated by their resistive switching (RS) behavior for emerging neuromorphic devices.

2 | Results and Discussion

The representative layered double perovskite model systems based on BNA and PDMA were synthesised by ball milling of the precursors based on $(PDMA)_2AgBiBr_8$ and $(BNA)_4AgBiBr_8$ compositions. While BNA-based double perovskites were previously known, PDMA ones are introduced for the first time [45, 46]. The powders were subsequently dissolved in the conventional solvent mixture of *N*,*N*-dimethylformamide and dimethyl sulfoxide and spin-coated to obtain thin films, as described in the Supporting Information. The structural properties of powders and thin films were analysed by X-ray diffraction (XRD) (Figure 3 and Figure S1) [45, 46]. In both powder XRD patterns (Figure S1), the perovskite phase can be identified alongside smaller quantities of unreacted precursors. The atomic-level structure was additionally analysed by solid-state NMR spectroscopy (Figures S2 and S3). For this purpose, the mechanosynthesized $(PDMA)_2AgBiBr_8$ and $(BNA)_4AgBiBr_8$ powders were compared with their respective pristine precursors ($(PDMA)Br_2$ and (BNA)Br, respectively). Comparison of the ^{13}C NMR spectra revealed noticeable shifts within the CH_2 range (40−50 ppm) and the aromatic region of the spacers (120−140 ppm), in addition to the presence of a new peak for BNA-based systems in the aromatic region. These variations suggest the presence of PDMA and BNA spacer cations in new chemical environments, signifying the emergence of new phases.

XRD patterns of the corresponding films exhibit distinctive (h00) reflections, indicating the parallel alignment relative to the substrate (Figure 3). This was particularly pronounced in the BNA-based system, displaying a slightly higher level of crystallinity than the PDMA-based one (Table S1). Both featured diffraction peaks at low angles of 2θ below 10°, which is associated with the (001) reflection and indicative of low-dimensional structures [43, 45, 46], with 7.7° for PDMA and 5.3° for BNA, corresponding

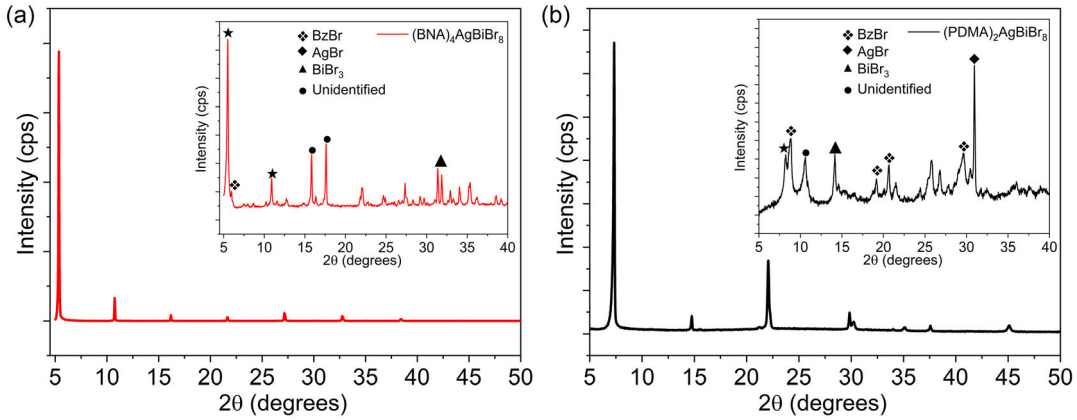

FIGURE 3 | XRD patterns of (a) RP and (b) DJ layered double perovskites based on $(BNA)_4AgBiBr_8$ and $(PDMA)_2AgBiBr_8$ compositions prepared mechanosynthetically (Figure S1) followed by solution processing of thin films on indium tin oxide (ITO) glass substrates. The corresponding powder XRD patterns are shown in the inset (stars indicating the perovskite phases), while further details are provided in the Supporting Information.

to d-spacings of 11.4 and 16.6 Å, respectively. Moreover, a comparison of the XRD patterns of films prepared by direct mixing of the precursors and the mechanosynthetic powders indicates a slightly higher level of crystallinity when using mechanochemistry (Figure S1). The structural analysis nonetheless suggests that the mechanochemical approach can be applied to prepare layered double perovskites and their films. The films were subjected to thermal and ambient atmosphere aging at 60%–70% relative humidity (Figure S4). While PDMABr-based system retained >90% of the intensity of its diffractions after 120 min at 100°C, BNABr-based system degraded after 30 min, leading to the formation of oxidised Ag phases, corroborating higher thermal stability of the DJ phases. In contrast, BNA-based RP systems exhibited longer shelf life as compared to DJ phases.

The morphology of the films was further investigated by scanning electron microscopy (Figure S5). The surface of the $(PDMA)_2AgBiBr_8$ films exhibited greater uniformity with larger domains, whereas $(BNA)_4AgBiBr_8$ featured a surface with randomly distributed regions with a higher concentration of Ag, as suggested by energy-dispersive X-ray elemental analysis, likely due to segregation that can be further optimised.

These structural and morphological features can significantly influence optoelectronic properties, which were analysed by UV-visible absorption and steady-state photoluminescence (PL) spectroscopy (Figure 4a,b). The presence of narrow excitonic absorption features at 415 nm for the PDMA-based perovskite and 410 nm for the BNA-based system indicates quantum and dielectric confinement effects characteristic of layered perovskites [47–49]. Furthermore, PL measurements showed signals at 510 and 515 nm for the PDMA and BNA systems, respectively, with a larger Stokes shift for BNA-based systems. The dynamics of photogenerated charge carriers were further assessed by time-resolved PL (TRPL) measurements (Figure 4c), which revealed a slightly faster decay in $(PDMA)_2AgBiBr_8$ films, exhibiting a second-order decay profile indicative of two radiative processes, i.e., PL quenching of free carriers and radiative recombination of trapped carriers [49]. This remained consistent for $(BNA)_4AgBiBr_8$ films, albeit with a longer average lifetime (τ) of 13 ns as compared to 6 ns for the $(PDMA)_2AgBiBr_8$, suggesting more promise in optoelectronics. Thin film preparation methodology can be further optimized for future applications.

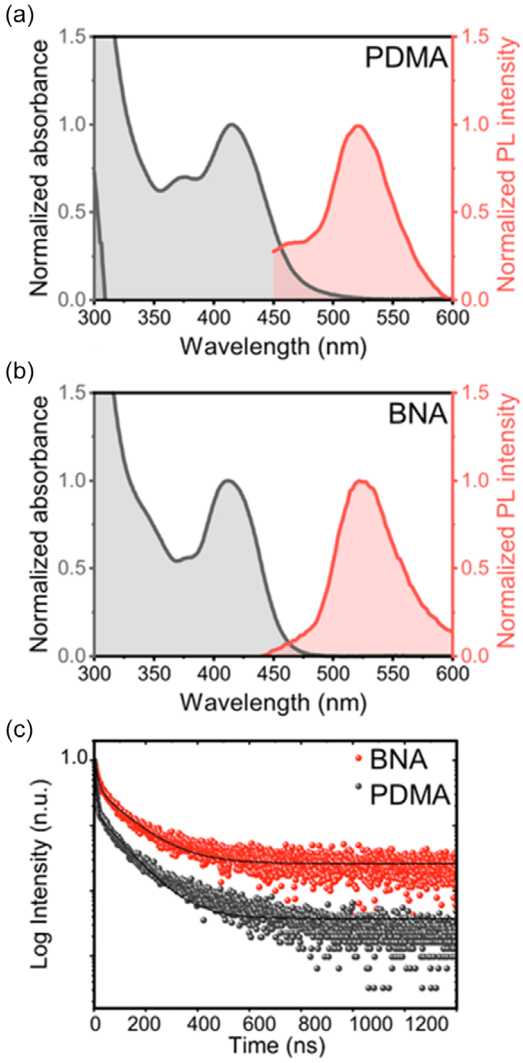

FIGURE 4 | (a,b) UV–vis absorption (left, grey) and PL spectra (right, red) for (a) PDMA- and (b) BNA-based layered double perovskite thin films. (c) Time-resolved PL spectra for PDMA (black) and BNA (red) layered double perovskites with the corresponding fits (black lines). The films were prepared on microscope glass and measured under ambient air. PL lifetimes were estimated assuming second-order decay profiles, as detailed in the experimental section of the Supporting Information.

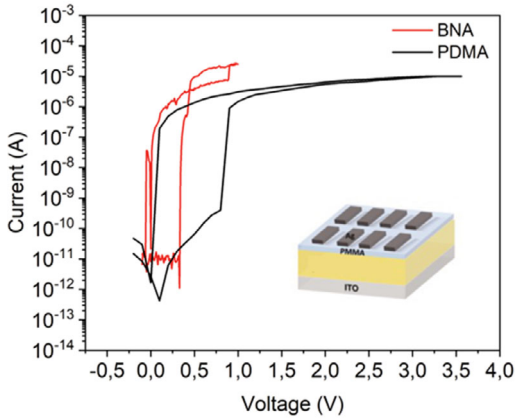

FIGURE 5 | Current–voltage characteristics of a two-terminal device (schematic shown in the inset) indicating RS for PDMA- (black) and BNA- (red) based layered double perovskite materials.

The potential of these materials in functional opto(electro)ionic technologies was further assessed in simplified two-terminal devices based on ITO/perovskite/poly(methyl metacrylate) (PMMA)/Ag configuration (Figure 5, inset). The perovskite precursor solution was spin-coated onto the bottom electrode, and a PMMA buffer layer was used to prevent excessive Ag diffusion to mitigate resistive switching (RS). The resulting devices were then tested without any precondition. Their current–voltage characteristics revealed RS properties in both RP and DJ compositions, featuring an abrupt high resistance states (HRS) to low resistance states switching upon biasing of the device (Figure 5). The abrupt switching was indicative of a filamentary-based RS mechanism rather than an interface-mediated switching that is characterized by a gradual transition. A commonly accepted mechanism for perovskite-based RS devices is the formation and rupture of conductive filaments formed by halide vacancies or metal cation migration [50, 51]. In this system, Ag and Br volatility were likely responsible for the RS, which is modulated by the low dimensionality of the hybrid double perovskites. This is of interest to the development of more energy-efficient and self-powered memory elements [50–52]. To this end, both compositions exhibited threshold RS behaviour with transient dynamics, where long-term information storage is not feasible. In general, memory systems based on ion migration can either store information, as in nonvolatile memories, or exhibit transient dynamics, where information cannot be retained after power removal, reflecting volatile switching. The volatile nature was reflected in the spontaneous decay of the current back to the HRS in the absence of bias, indicating carrier/ionic accumulation upon biasing and a diffusion back process at near-zero bias. While the threshold voltage in the case of the BNA system appeared to be at ≈300 mV, the PDMA system threshold was at 800 mV. Such low switching voltage (<1 V) highlights the potential of these layered perovskites for low-power memory applications. Furthermore, in both cases, the RS behaviour could be obtained without any electroforming step, an important property for designing memory systems. To this end, both systems exhibited a high ON/OFF ratio of ≈5 orders of magnitude (10^5), showcasing the potential for neuromorphic computing. Future work on these systems will provide more insights into their mechanisms of operation, dynamics, and potential applications.

3 | Conclusion

In summary, we demonstrate the use of mechanosynthesis in layered lead-free double perovskites to assemble benzylammonium (BNA)-based RP and 1,4-phenylenedimethylammonium (PDMA)-based DJ bromide double perovskites. XRD patterns of the corresponding powders and thin films confirmed the distinct low-dimensional and layered structures, with a slightly higher level of crystallinity for samples prepared mechanosynthetically. Moreover, optoelectronic characterisation, including UV–vis absorption and PL spectroscopy, showcased excitonic behaviour in both systems, with a faster TRPL decay in the PDMA-based case. Finally, the materials were applied to resistive switching memories, showcasing their potential for emerging neuromorphic systems, which require further investigation. These findings underscore the utility of mechanosynthesis to access layered halide double perovskites, opening a path for their future use in perovskite-based thin-film technologies .

Author Contributions

Gianluca Bravetti: performed the early experimental work and analysis, and wrote the first manuscript. **Maryam Ghasemi**: performed complementary synthesis and structural analysis under the supervision of **Mohammad Reza Golobostanfard** and **Jovana V. Milić**, while **Michalis Loizos** and **Marinos Tountas** analysed resistive switching under the supervision of **Konstantinos Rogdakis** and **Emmanuel Kymakis**. The complementary analysis of resistive switches was performed under the supervision of **Mahesh Kumar** and **Jovana V. Milić**, while **Ghewa AlSabeh** performed time-resolved PL and NMR spectroscopy under the supervision of **Jovana V. Milić**. All authors discussed and contributed to the manuscript.

Acknowledgments

G.B. and J.V.M. appreciate the support of DFG-SPP project 186453 and the Swiss National Science Foundation (SPARK project no. 221017) for enabling preliminary work, as well as Prof. Ullrich Steiner at the Adolphe Merkle Institute for his support over the years. J.V.M. further appreciates the support from the Swiss Leading House for South Asia through the partnership grant with M.K., and especially the talented young researcher, Mubashir M. Ganaie, whose work has contributed significantly to the continuation of these research developments. M.M., M.R.G., and J.V.M. are grateful to the Research Council of Finland (project no. 362642) for supporting this research, and J.V.M. and M.R.G. further acknowledge the support by the European Research Council under the EU Horizon innovation program (grant agreement no. 101114653, SmartHyMat). The research project is implemented within the framework of the H.F.R.I. call "Basic Research Financing (Horizontal Support of All Sciences)" under the National Recovery and Resilience Plan "Greece 2.0," funded by the European Union – NextGenerationEU (H.F.R.I. Project Number: 14728) and with the support from the European Union's Horizon 2020 research and innovation program under project INFRACHIP (grant agreement no. 101131822), and project ELEGANCE (grant agreement no. 101161114) for which M.L., M.T., K.R., and E.K. are grateful. The authors also acknowledge the support of Dr. Felix Eickemeyer at the Laboratory of Photonics and Interfaces (LPI) at EPFL in Switzerland for performing the PL and TRPL measurements, Dr. Masaud Almalki for his support in the analysis (LPI, EPFL), and Dr. Laura Piveteau (ISIC-NMRP, EPFL) and Rémy Lucien Michel Fontaine for support with NMR spectroscopy.

Open access publishing facilitated by Turun yliopisto, as part of the Wiley - FinELib agreement.

Conflicts of Interest

The authors declare no conflicts of interest.

Data Availability Statement

Data can be accessed at the https://doi.org/10.5281/zenodo.18922192 and it is available under the license CC-BY-4.0 (Creative Commons Attribution-ShareAlike 4.0 International).

References

1. A. K. Jena, A. Kulkarni, and T. Miyasaka, "Halide Perovskite Photovoltaics: Background, Status, and Future Prospects," *Chemical Reviews* 119 (2019): 3036–3103.

2. W. S. Yang, B.-W. Park, E. H. Jung, et al., "Iodide Management in Formamidinium-Lead-Halide–based Perovskite Layers for Efficient Solar Cells," *Science* 356 (2017): 1376–1379.

3. S. D. Stranks, G. E. Eperon, G. Grancini, et al., "Electron-Hole Diffusion Lengths Exceeding 1 Micrometer in an Organometal Trihalide Perovskite Absorber," *Science* 342 (2013): 341–344.

4. M. M. Lee, J. Teuscher, T. Miyasaka, T. N. Murakami, and H. J. Snaith, "Efficient Hybrid Solar Cells Based on Meso-Superstructured Organometal Halide Perovskites," *Science* 338 (2012): 643–647.

5. D. Zhang, D. Li, Y. Hu, A. Mei, and H. Han, "Degradation Pathways in Perovskite Solar Cells and How to Meet International Standards," *Communications Materials* 3 (2022): 58.

6. T. A. Berhe, W.-N. Su, C.-H. Chen, et al., "Organometal Halide Perovskite Solar Cells: Degradation and Stability," *Energy & Environmental Science* 9 (2016): 323–356.

7. R. Wang, M. Mujahid, Y. Duan, Z. Wang, J. Xue, and Y. Yang, "A Review of Perovskites Solar Cell Stability," *Advanced Functional Materials* 29 (2019): 1808843.

8. M. Degani, Q. An, M. Albaladejo-Siguan, et al., "23.7% Efficient Inverted Perovskite Solar Cells by Dual Interfacial Modification," *Science Advances* 7 (2021): 7930.

9. M. Awais, D. Thrithamarassery Gangadharan, F. Tan, and M. I. Saidaminov, "How to Make 20% Efficient Perovskite Solar Cells in Ambient Air and Encapsulate Them for 500 Hr of Operational Stability," *Chemistry of Materials* 34 (2022): 8112–8118.

10. S. Ma, G. Yuan, Y. Zhang, N. Yang, Y. Li, and Q. Chen, "Development of Encapsulation Strategies towards the Commercialization of Perovskite Solar Cells," *Energy & Environmental Science* 15 (2022): 13–55.

11. F. Bisconti, M. Leoncini, G. Bravetti, et al., "Blocking Wide Bandgap Mixed Halide Perovskites' Decomposition through Polymer Inclusion," *Journal of Materials Chemistry C* 11 (2023): 12213–12221.

12. N. Taurisano, G. Bravetti, S. Carallo, et al., "Inclusion of 2D Transition Metal Dichalcogenides in Perovskite Inks and Their Influence on Solar Cell Performance," *Nanomaterials* 11 (2021): 1706.

13. F. Giustino and H. J. Snaith, "Toward Lead-Free Perovskite Solar Cells," *ACS Energy Letters* 1 (2016): 1233–1240.

14. G. Flora, D. Gupta, and A. Tiwari, "Toxicity of Lead: A Review with Recent Updates," *Interdisciplinary Toxicology* 5 (2012): 47–58.

15. R.-T. Wen, C. G. Granqvist, and G. A. Niklasson, "Eliminating Degradation and Uncovering Ion-Trapping Dynamics in Electrochromic WO3 Thin Films," *Nature Materials* 14 (2015): 996–1001.

16. Y. Gao, Y. Pan, F. Zhou, G. Niu, and C. Yan, "Lead-Free Halide Perovskites: A Review of the Structure–property Relationship and Applications in Light Emitting Devices and Radiation Detectors," *Journal of Materials Chemistry A* 9 (2021): 11931–11943.

17. S. Ghosh, H. Shankar, and P. Kar, "Recent Developments of Lead-Free Halide Double Perovskites: A New Superstar in the Optoelectronic Field," *Materials Advances* 3 (2022): 3742–3765.

18. J. Li, J. Duan, X. Yang, Y. Duan, P. Yang, and Q. Tang, "Review on Recent Progress of Lead-Free Halide Perovskites in Optoelectronic Applications," *Nano Energy* 80 (2021): 105526.

19. J. Li, H.-L. Cao, W.-B. Jiao, et al., "Biological Impact of Lead from Halide Perovskites Reveals the Risk of Introducing a Safe Threshold," *Nature Communications* 11 (2020): 310.

20. H. Fu, "Review of Lead-Free Halide Perovskites as Light-Absorbers for Photovoltaic Applications: From Materials to Solar Cells," *Solar Energy Materials and Solar Cells* 193 (2019): 107–132.

21. N. K. Tailor, A. Listorti, S. Colella, and S. Satapathi, "Lead-Free Halide Double Perovskites: Fundamentals, Challenges, and Photovoltaics Applications," *Advanced Materials Technologies* 8 (2022): 2200442.

22. F. Igbari, Z.-K. Wang, and L.-S. Liao, "Progress of Lead-Free Halide Double Perovskites," *Advanced Energy Materials* 9 (2019): 1803150.

23. P. Zhang, J. Yang, and S.-H. Wei, "Manipulation of Cation Combinations and Configurations of Halide Double Perovskites for Solar Cell Absorbers," *Journal of Materials Chemistry A* 6 (2018): 1809–1815.

24. G. Volonakis, M. R. Filip, A. A. Haghighirad, et al., "Lead-Free Halide Double Perovskites via Heterovalent Substitution of Noble Metals," *The Journal of Physical Chemistry Letters* 7 (2016): 1254–1259.

25. A. H. Slavney, T. Hu, A. M. Lindenberg, and H. I. Karunadasa, "A Bismuth-Halide Double Perovskite with Long Carrier Recombination Lifetime for Photovoltaic Applications," *Journal of the American Chemical Society* 138 (2016): 2138–2141.

26. E. T. McClure, M. R. Ball, W. Windl, and P. M. Woodward, "Cs_2AgBiX_6 (X = Br, Cl): New Visible Light Absorbing, Lead-Free Halide Perovskite Semiconductors," *Chemistry of Materials* 28 (2016): 1348–1354.

27. H. Lei, D. Hardy, and F. Gao, "Lead-Free Double Perovskite $Cs_2AgBiBr_6$: Fundamentals, Applications, and Perspectives," *Advanced Functional Materials* 31 (2021): 2105898.

28. C. N. Savory, A. Walsh, and D. O. Scanlon, "Can Pb-Free Halide Double Perovskites Support High-Efficiency Solar Cells?," *ACS Energy Letters* 1 (2016): 949–955.

29. N. Rajeev Kumar and R. Radhakrishnan, "Electronic, Optical and Mechanical Properties of Lead-Free Halide Double Perovskites Using First-Principles Density Functional Theory," *Materials Letters* 227 (2018): 289–291.

30. M. T. Sirtl, R. Hooijer, M. Armer, et al., "2D/3D Hybrid $Cs_2AgBiBr_6$ Double Perovskite Solar Cells: Improved Energy Level Alignment for Higher Contact-Selectivity and Large Open Circuit Voltage," *Advanced Energy Materials* 12 (2022): 2103215.

31. E. G. Tulsky and J. R. Long, "Dimensional Reduction: A Practical Formalism for Manipulating Solid Structures," *Chemistry of Materials* 13 (2001): 1149–1166.

32. C. C. Stoumpos, C. M. M. Soe, H. Tsai, et al., "High Members of the 2D Ruddlesden-Popper Halide Perovskites: Synthesis, Optical Properties, and Solar Cells of $(CH_3(CH_2)_3NH_3)2(CH_3NH_3)_4Pb_5I_{16}$," *Chem* 2 (2017): 427–440.

33. L. Mao, R. M. Kennard, B. Traore, et al., "Seven-Layered 2D Hybrid Lead Iodide Perovskites," *Chem* 5 (2019): 2593–2604.

34. B. A. Connor, L. Leppert, M. D. Smith, J. B. Neaton, and H. I. Karunadasa, "Layered Halide Double Perovskites: Dimensional Reduction of $Cs_2AgBiBr_6$," *Journal of the American Chemical Society* 140 (2018): 5235–5240.

35. L.-Y. Bi, Y.-Q. Hu, M.-Q. Li, et al., "Two-Dimensional Lead-Free Iodide-Based Hybrid Double Perovskites: Crystal Growth, Thin-Film

Preparation and Photocurrent Responses," *Journal of Materials Chemistry A* 7 (2019): 19662–19667.

36. M. Ghasemi, P. Karcili, A. Mishra, M. R. Golobostanfard, and J. V. Milić, "Molecular Engineering of Layered Halide Double Perovskites: Challenges and Opportunities in Optoelectronics and Beyond," *Advanced Energy Materials* 15 (2025): 2502693.

37. A. Jana, M. Mittal, A. Singla, and S. Sapra, "Solvent-Free, Mechanochemical Syntheses of Bulk Trihalide Perovskites and Their Nanoparticles," *Chemical Communications* 53 (2017): 3046–3049.

38. D. Prochowicz, M. Franckevičius, A. M. Cieślak, S. M. Zakeeruddin, M. Grätzel, and J. Lewiński, "Mechanosynthesis of the Hybrid Perovskite $CH_3NH_3PbI_3$: Characterization and the Corresponding Solar Cell Efficiency," *Journal of Materials Chemistry A* 3 (2015): 20772–20777.

39. D. Prochowicz, P. Yadav, M. Saliba, et al., "Mechanosynthesis of Pure Phase Mixed-Cation $MA_xFA_{1-x}PbI_3$ Hybrid Perovskites: Photovoltaic Performance and Electrochemical Properties," *Sustainable Energy & Fuels* 1 (2017): 689–693.

40. D. J. Kubicki, D. Prochowicz, A. Hofstetter, et al., "Formation of Stable Mixed Guanidinium–Methylammonium Phases with Exceptionally Long Carrier Lifetimes for High-Efficiency Lead Iodide-Based Perovskite Photovoltaics," *Journal of the American Chemical Society* 140 (2018): 3345–3351.

41. D. Prochowicz, M. Saski, P. Yadav, M. Grätzel, and J. Lewiński, "Mechanoperovskites for Photovoltaic Applications: Preparation, Characterization, and Device Fabrication," *Accounts of Chemical Research* 52 (2019): 3233–3243.

42. P. Ferdowsi, E. Ochoa-Martinez, U. Steiner, and M. Saliba, "One-Step Solvent-Free Mechanochemical Incorporation of Insoluble Cesium Salt into Perovskites for Wide Band-Gap Solar Cells," *Chemistry of Materials* 33 (2021): 3971–3979.

43. H. J. Jöbsis, L. A. Muscarella, M. Andrzejewski, N. P. M. Casati, and E. M. Hutter, "Mechanochemical Formation Mechanism of Alloyed AgBi-Elpasolites," *Journal of the American Chemical Society* 147 (2025): 24519–24526.

44. M. Mladenović, F. Jahanbakhshi, J.-H. Im, et al., "Silver Bismuth Iodides for Photovoltaic Applications: Insights from Ab Initio Calculations and Experimental Analysis," *ACS Applied Energy Materials* 8 (2025): 7424.

45. Y. Li, J. V. Milić, A. Ummadisingu, et al., "Bifunctional Organic Spacers for Formamidinium-Based Hybrid Dion–Jacobson Two-Dimensional Perovskite Solar Cells," *Nano Letters* 19 (2019): 150–157.

46. Y.-R. Wang, A. Senocrate, M. Mladenović, et al., "Photo De-Mixing in Dion-Jacobson 2D Mixed Halide Perovskites," *Advanced Energy Materials* 12 (2022): 2200768.

47. A. Simbula, L. Wu, F. Pitzalis, et al., "Exciton Dissociation in 2D Layered Metal-Halide Perovskites," *Nature Communications* 14 (2023): 4125.

48. Z. Gan, Y. Cheng, W. Chen, K. P. Loh, B. Jia, and X. Wen, "Photophysics of 2D Organic–Inorganic Hybrid Lead Halide Perovskites: Progress, Debates, and Challenges," *Advancement of Science* 8 (2021): 2001843.

49. J.-C. Blancon, J. Even, C. C. Stoumpos, M. G. Kanatzidis, and A. D. Mohite, "Semiconductor Physics of Organic–inorganic 2D Halide Perovskites," *Nature Nanotechnology* 15 (2020): 969–985.

50. M. M. Ganaie, G. Bravetti, S. Sahu, M. Kumar, and J. V. Milić, "Resistive Switching in Benzylammonium-Based Ruddlesden–Popper Layered Hybrid Perovskites for Non-Volatile Memory and Neuromorphic Computing," *Materials Advances* 5 (2024): 1880.

51. M. Loizos, K. Rogdakis, W. Luo, et al., "Resistive Switching Memories with Enhanced Durability Enabled by Mixed-Dimensional Perfluoroarene Perovskite Heterostructures," *Nanoscale Horizons* 9 (2024): 1146.

52. K. Rogdakis, M. Loizos, G. Viskadouros, and E. Kymakis, "Memristive Perovskite Solar Cells towards Parallel Solar Energy Harvesting and Processing-in-Memory Computing," *Materials Advances* 3 (2022): 7002.

Supporting Information

Additional supporting information can be found online in the Supporting Information section. **Supporting Fig. S1**: XRD patterns of (a,b) mechanosynthetic powders and (c,d) thin films of Ruddlesden-Popper (a,c) and Dion-Jacobson (b,d) layered double perovskites with (WM) and without (WOM) mechanosynthesis based on $(BNA)_4AgBiBr_8$ and $(PDMA)_2AgBiBr_8$ compositions. Powder XRD patterns of the precursors (AgBr, $BiBr_3$, BNABr, and $PDMABr_2$) are included for comparison. **Supporting Fig. S2**: $^1H \rightarrow {}^{13}C$ cross-polarization (CP) magic angle spinning (MAS) NMR spectra at 298 K for the pure spacer $(PDMA)Br_2$ precursor and mechanosynthetic $(PDMA)_2AgBiBr_8$. **Supporting Fig. S3**: $^1H \rightarrow {}^{13}C$ cross-polarization (CP) magic angle spinning (MAS) NMR spectra at 298 K for the pure spacer (BNA)Br precusor and mechanosynthetic $(BNA)_4AgBiBr_8$. **Supporting Fig. S4**: XRD patterns of (a) $(BNA)_4AgBiBr_8$ and (b) $(PDMA)_2AgBiBr_8$ systems after thermal stress at 100°C, measured every 30 min at ambient air (60–70% relative humidity) over a period of 120 min. (c) $(BNA)_4AgBiBr_8$ and (d) $(PDMA)_2AgBiBr_8$ systems shelf-life stability (inside a glovebox under nitrogen). **Supporting Fig. S5**: SEM images with respective EDX mapping for $(PDMA)_2AgBiBr_8$ (left) and $(BNA)_4AgBiBr_8$ (right) thin films on ITO, highlighting Ag (green) and Bi (red) element maps, with the superimposed maps of investigated elements (top). **Supporting Table S1**: Full width at half maximum (FWHM) and crystallite size of PDMA and BNA-based systems using mechanosynthesis (WM). **Supporting Table S2**: Full width at half maximum (FWHM) and crystallite size of PDMA and BNA-based systems without using mechanosynthesis (WOM).